Electromagnetic Analysis of Dielectric Shimming using High Permittivity Materials

Wyger Brink[1] and Andrew Webb[1]
[1]Radiology, Leiden University Medical Center, Leiden, Netherlands, Zuid-Holland, Netherlands

Target audience: Researchers and RF engineers interested in RF shimming at high fields using dielectric materials.

Purpose: To present an electromagnetic analysis of dielectric shimming using high permittivity materials at 7T.

Methods: In vivo B_1^+ maps were acquired in the brain using the DREAM method [1] on a Philips Achieva 7T MRI system (Philips Healthcare, Best, The Netherlands) equipped with a quadrature birdcage transmit coil and a 32-channel receive array (Nova Medical, Wilmington, MA). The maps were acquired without and with a single dielectric pad at the left side of the head. The dielectric pad had a size of 18 x 18 x 0.8 cm^3 and consisted of a suspension of either calcium titanate powder ($\varepsilon_r \approx 110$) [2] or barium titanate powder ($\varepsilon_r \approx 290$) [3].

Electromagnetic simulations of the B_1^+ field were performed in xFDTD (Remcom inc., State College, PA, USA) with a numerical model of the transmit head coil loaded with Virtual Family member 'Duke' [4].

The "secondary" field (B_2^+) was determined in the simulated dataset by complex subtraction of the B_1^+ field without pad (the "primary" field) from the B_1^+ field simulated with pad. Normalization of the field data was to a unit current in the coil. A first-order approximation of the secondary magnetic field was made using the integral form of Maxwell's equations and is expressed as

$$\hat{\boldsymbol{B}}_2 = \mathrm{j}\omega\varepsilon_0\mu_0 \int_D \nabla g(\boldsymbol{x}-\boldsymbol{x}') \times \chi_e(\boldsymbol{x}')\boldsymbol{E}(\boldsymbol{x}')\mathrm{d}V \qquad (1)$$

which represents the field that would be radiated in free space by the currents induced in the dielectric. More information on this formulation can be found in [5].

Results: Figure 1 presents the measured (top) and simulated (bottom) B_1^+ maps for the three configurations which shows a strong asymmetry in the B_1^+ field when going to a higher permittivity material (indicated with the arrow). Figure 2 shows the secondary field analysis with its amplitude (top) and phase difference with respect to the primary field (bottom). These maps show that the CaTiO$_3$ pad introduces a secondary field with a symmetric amplitude distribution and a relatively small (<70º) and uniform phase difference, which results in a symmetric B_1^+ distribution. The secondary field introduced by the BaTiO$_3$ pad shows to be much larger and asymmetric in both its amplitude and phase distribution, with phase differences reaching almost 160º close to the dielectric (see arrow). Given the complex nature of electromagnetic fields, both factors are required for describing the strong field null indicated by the arrows in figure 1.

Figure 3 illustrates the magnitude of the induced current density (top), which shows that the current distribution is rather uniform in the CaTiO$_3$ pad, but is asymmetric in the BaTiO$_3$ pad. The first order approximation of the B_2^+ field (bottom), using Eq. (1), reflects that the asymmetry is to some degree related to this asymmetric current distribution. Other factors may include sample loading of the secondary field, which is not incorporated here.

Discussion: The effect of introducing a dielectric material can be interpreted as introducing displacement currents that produce a secondary field. For low values of the permittivity, this leads to a coherent increase in B_1^+ near the pad resulting in a symmetric elevation of B_1^+. For higher values of the permittivity however, areas of low B_1^+ can arise even next to the dielectric pad, resulting in an asymmetric B_1^+ distribution. These effects cannot be described using a simple plane wave analysis [6] or ampere's law [7]. The current analysis shows that the phase and amplitude of the secondary field need to be considered for describing this asymmetry and this requires prior knowledge of the induced current distribution in the dielectric and the inclusion of dielectric properties of the sample. These results provide further insight that can be used in the design of dielectric shims for optimized shimming performance.

Conclusion: In this work, the field patterns resulting from a high permittivity pad at 7T have been analyzed and a theoretical framework for describing these effects has been evaluated.

References: [1] Nehrke et al., *MRM 2012*, 68:1517–1526; [2] Teeuwisse et al., *MRM 2012*, 67:1285–1293; [3] Teeuwisse et al., *MRM 2012*, 67:912–918; [4] Christ et al., Phys Med Biol 2010, 55:N23–N38.; [5] Jin, *Crc Press, 1999*; [6] Ketterman et al., *Proc. ISMRM 2012*, 2699; [7] Luo et al., *MRM 2012*, DOI 10.1002/mrm.24433.
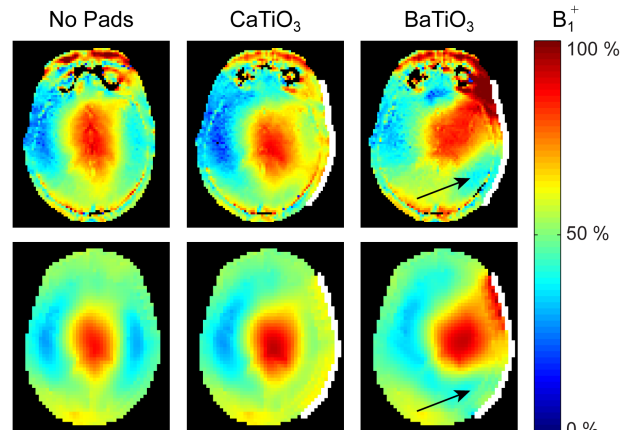
Figure 1. Measured (top) and simulated (bottom) transverse B_1^+ maps having no pads in place (left), a single dielectric pad (in white) with a suspension of CaTiO$_3$ (middle) or BaTiO$_3$ (right).
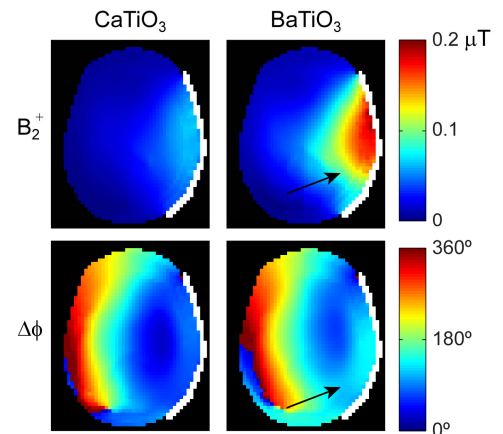

Figure 2. Secondary field B_2^+ amplitude (top) and phase difference with respect to the primary B_1^+ field (bottom) for the two dielectric pads.
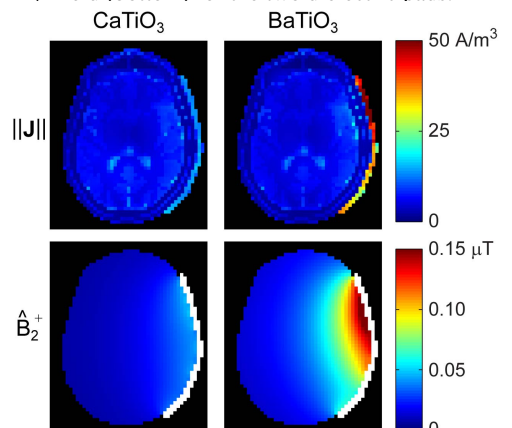

Figure 3. Transverse maps of the induced current magnitude (top) and first order approximation of the secondary field amplitude (bottom).